LANGMUIR

pubs.acs.org/Langmuir Article

Self-Assembled Bio-Organometallic Nanocatalysts for Highly Enantioselective Direct Aldol Reactions

Xuejiao Yang,[⊥] Liwei Zhang,[⊥] Yaoyu Liang,[⊥] Yuefei Wang,* Yuhe Shen, Qiguo Xing, Wei Qi, Pengfei Wang, Xiao Liu, Mengyao Yang, Rongxin Su, Mingxia He, and Zhimin He

Cite This: https://dx.doi.org/10.1021/acs.langmuir.0c01485 Read Online

ACCESS | Metrics & More | Article Recommendations | Supporting Information

ABSTRACT: Supramolecular nanocatalysts were designed for asymmetric reactions through the self-assembly process of a bio-organometallic molecule, ferrocene-L-prolinamide (Fc-CO-NH-P). Fc-CO-NH-P could self-assemble into versatile nanostructures in water, including nanospheres, nanosheets, nanoflowers, and pieces. In particular, the self-assembled nanoflowers exhibited a superior specific surface area, high stability, and delicate three-dimensional (3D) chiral catalytic active sites. The nanoflowers could serve as heterogeneous catalysts with an excellent catalytic performance toward direct aldol reactions in aqueous solution, achieving both high yield (>99%) and stereoselectivity (anti/syn = 97:3, ee% >99%). This study proposed a significant strategy to fabricate supramolecular chiral catalysts, serving as a favorable template for designing new asymmetric catalysts.

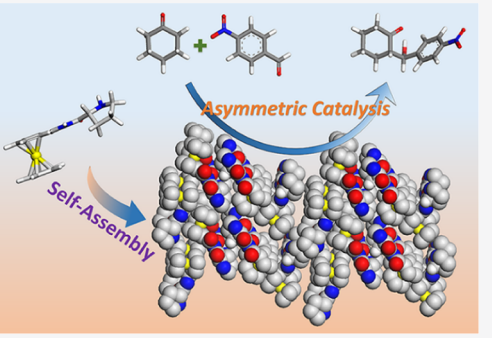

INTRODUCTION

Enzymes promote various chemical reactions through folding into three-dimensional ordered structures, by acting specifically with reactants, giving a high efficiency and selectivity. L-Proline was regarded as the simplest aldolase.[1−3] It has been studied in many chemical reactions, for instance, intermolecular aldol reactions, Michael addition reactions, Diels−Alder reactions, and others.[4−8] Aldol condensation is a kind of crucial C−C bond formation reaction, increasing the diversity and complexity of the molecules, and is applied in processing industry widely. L-Proline is a highly efficient catalyst for aldol reactions in organic solvents, while it is a poor catalyst in water.[9,10] However, in view of the environment, safety, and cost, carrying out aldol reactions in aqueous solutions with both high conversion and stereoselectivity is highly desired.[10,11]

The design of a highly enantioselective chiral catalyst has been a long-standing challenge.[12−15] One of the strategies is creating steric confinements at the catalytic site of an organic catalyst by mimicking enzymes. Ferrocene has a large size and special spatial configuration relative to other functional groups. Ferrocene derivatives with planar chirality are of great importance in asymmetric catalysis, resulting in high stereoselectivity.[16,17] However, the commonly used ferrocene-modified catalysts are a kind of single organic molecule. Recently, chiral catalysts have been designed for asymmetric reactions on DNA,[18−20] polymers,[21,22] nanoparticles,[23,24] cellulose nanocrystals,[25] metal−organic frameworks,[26,27] and others. Moreover, enzyme-mimicking supramolecular nanostructures based on self-assembly of simple peptides and amino acids have drawn increasing attention and have been applied in asymmetric reactions widely.[28−35] Therefore, it is promising to develop supramolecular nanocatalysts for asymmetric reactions by self-assembly of ferrocene-modified biomolecules, thereby achieving higher conversion, stereoselectivity, and reusability.

Herein, we designed a bio-organometallic catalyst, ferrocene-L-prolinamide (Fc-CO-NH-P), by combining ferrocene, the functional group providing steric hindrance and stereoselectivity in the self-assembly,[36−39] with a cheap amino acid derivative (L-prolinamide) (Scheme S1 and Figures S1−S4). Fc-CO-NH-P could self-assemble into versatile nanostructures, including nanospheres, sheets, nanoflowers, and pieces (Scheme 1a). The morphology of nanostructures was related to the catalytic activity toward direct aldol reactions. Specifically, the nanoflowers exhibited sufficient catalytic sites and a chiral microstructure (Scheme 1b), which could serve as heterogeneous catalysts with superior catalytic activity and selectivity toward direct aldol reactions in aqueous media (Scheme 1c).

RESULTS AND DISCUSSION

The preparation of versatile supramolecular nanostructures was performed by a "heating−cooling" strategy. Fc-CO-NH-P (1 mg) was dissolved in 1 mL of phosphate buffer and sodium

Received: May 19, 2020
Revised: October 20, 2020

Scheme 1. (a) Fc-CO-NH-P Self-Assembled into Three-Dimensional (3D) Nanoflowers; (b) Proposed Chiral Configuration of Fc-CO-NH-P Molecules within the Nanoflowers; and (c) 3D Nanoflower-catalyzed Direct Aldol Reaction in Aqueous Solution

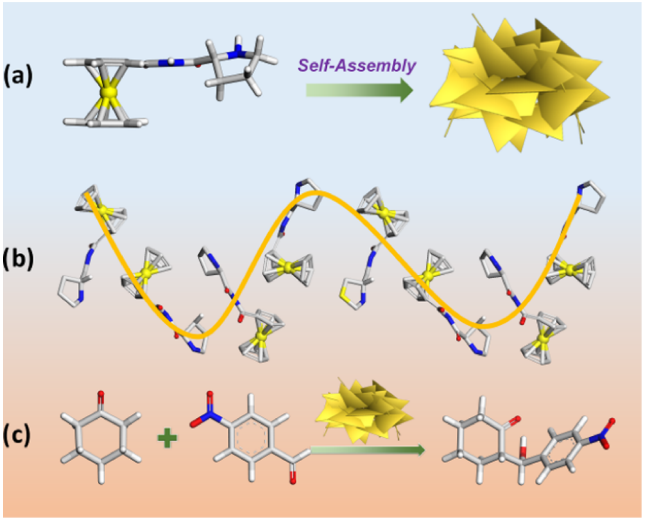

hydroxide solution (50 mM; pH 6.0, 7.0, 9.0, 12.0) at 60 °C, respectively. After being fully dissolved, the samples were moved to a water bath at 25 °C for 24 h to achieve full self-assembly. After self-assembly, the nanostructures were separated at the bottom of the tubes, and the formed self-assemblies were named P6, P7, P9, and P12 for phosphate buffer with different pHs and N6, N7, N9, and N12 for sodium hydroxide solution with different pHs. Using high-magnification transmission electron microscopy (TEM), scanning electron microscopy (SEM), and atomic force microscopy (AFM), we studied the morphology of the nanostructures. P6 consisted of nanospheres with a diameter of 148.5 nm (Figure S5a–c), derived from DLS. Huge microsheets were observed in P7 and P9, with several microns in length and a thickness of ~50 nm (Figures S5d–f, S6a, S7a, and 1a–c). Intriguingly, three-dimensional (3D) flower-like nanostructures were formed in P12. The nanoflowers were formed by twirling and stacking of multiple layers with a thickness of 11.85 nm (Figures 1d–f and S6b, S7b, S8). The diameter of the whole flower was about 900 nm, and its height was 400 nm. N12 was made of small flat pieces with a length of 500 nm and a height of 8 nm (Figures 1g–i and S6c, S7c). However, no ordered structures were found in N6, N7, and N9. It is worth noting that the TEM images with selected area electron diffraction (SAED) patterns at high resolution indicated that P9, P12, and N12 exhibited an ordered crystal structure, with a lattice spacing of 2.8, 2.5 and 2.6, and 3.5 Å, respectively (Figure 1c,f,i, and insets).

For a deeper understanding of the supramolecular nanostructures, we investigated the secondary structure using Fourier transform infrared (FTIR) spectroscopy. In the N–H stretching band, the nanostructures showed a similar broad and strong peak at 3425 cm^{-1} (Figure 2a), corresponding to the free amide groups,[37] and in the amide I region, P7, P9, and P12 showed a primary peak located at 1635 cm^{-1} (Figure 2b), which was in agreement with a hydrogen-bonded carbonyl group. Although the nanospheres, sheets, and nanoflowers exhibited different morphologies, the intermolecular hydrogen

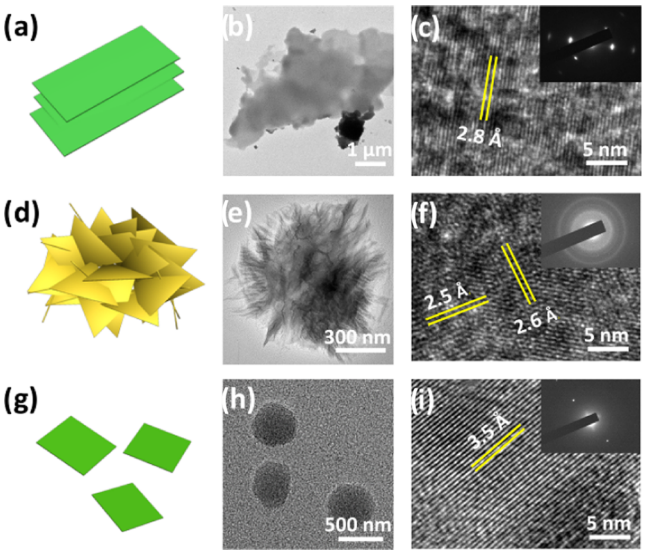

Figure 1. Schematic diagram: TEM images of (a–c) P9, (d–f) P12, and (g–i) N12. The high-resolution TEM images displayed the crystal lattices (c, f, i) and the corresponding selected area electron diffraction (SAED) patterns (insets).

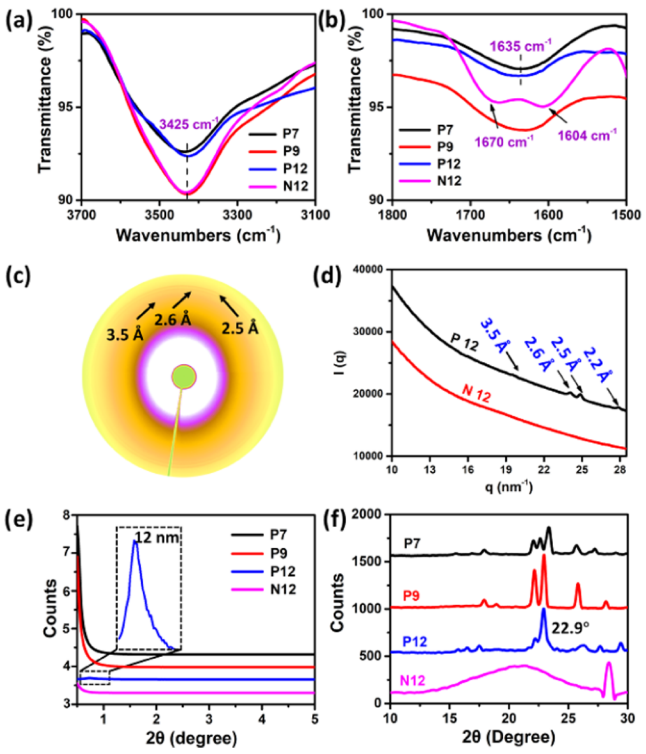

Figure 2. FTIR spectra of the (a) N–H stretching bands and (b) carbonyl stretching vibration mode of amino acid residues. (c) Two-dimensional (2D) WAXD pattern of nanoflowers. (d) WAXD 1D profiles of P12 and N12. (e) Small-angle and (f) wide-angle X-ray powder diffractograms of P7, P9, P12, and N12.

bonds were similar. Furthermore, the characteristic absorption peak located at 1670 cm^{-1} for N12, suggesting that the hydrogen bond was different from those of the other nanostructures, and the peak at 1604 cm^{-1} corresponded to the stretching vibration of C=C. These characteristic peaks suggested that the amido bonds of Fc-CO-NH-P were involved in the formation of different nanostructures. Furthermore, to

https://dx.doi.org/10.1021/acs.langmuir.0c01485
Langmuir XXXX, XXX, XXX–XXX

probe the packing mode of Fc-CO-NH-P within the self-assemblies, we performed in situ synchrotron wide-angle X-ray diffraction (WAXD). The nanoflowers showed obvious reflections corresponding to *d* spacings of 2.2, 2.5, 2.6, and 3.5 Å (Figure 2c,d), which was consistent with the SAED patterns. These reflections were ascribed to the ordered alignment between adjacent Fc moieties.[40−43] However, in other self-assemblies, there were no obvious reflections (Figures 2d and S9). The results indicated that compared with other self-assemblies, the molecular arrangement of nanoflowers was more ordered. Small-angle X-ray diffraction was further used to investigate the crystal structure. As shown in Figure 2e, only P12 exhibited the spike corresponding to the *d* spacing of 12 nm, which was exactly consistent with the thickness of the petals in 3D nanoflowers. At a wider angle, both the sheets and nanoflowers had a diffraction peak at 2θ values of 22.9°, indicating the *d* spacing of 3.88 Å, which could be attributed to the strong $\pi-\pi$ packing interactions (Figure 2f).

Furthermore, the terahertz spectra were used to study the intermolecular forces of self-assemblies. The nanoflowers showed three peaks at 3.9, 5.8, and 7.6 THz. These peaks may be caused by the intermolecular hydrogen bond between neighboring residues.[44−47] However, for self-assembled pieces, no obvious peak was observed (Figure 3). The differences in

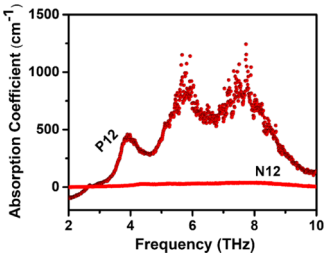

Figure 3. Terahertz spectrum of P12 and N12.

terahertz spectra revealed that the intermolecular hydrogen bonding was significantly different, leading to the formation of diverse morphologies. Combining the FTIR spectra, in situ WAXD, powder XRD, and terahertz spectra, we proved that the self-assembled nanoflowers had a delicate and ordered crystalline structure, in which the hydrogen bonds and $\pi-\pi$ stacking played a vital role.

According to the obtained structural information from multiple characterizations, a hypothetical unit cell for the self-assembled nanoflower was proposed[48] and then optimized by density functional theory (DFT) calculations. The designed triclinic cell contained four Fc-CO-NH-P molecules (Figure 4a). Each two molecules were interacted by $\pi-\pi$ stacking interactions between the Fc groups (Figure S10a), while the pyrrolidine groups were located at the face of *bc* (Figure S11). Among the neighboring cells, the $\pi-\pi$ packing interactions (Figure S10b) and the hydrogen bonds between CO···NH (Figure S10c) played a crucial role in stabilizing the structure. Along the *c*-axis, the Fc-CO-NH-P molecules exhibited an apparent chiral arrangement, and the Fc moieties were orderly arranged into a uniform array, exhibiting *d* spacings of 2.6 and 3.5 Å (Figure 4b), which was in line with the TEM images, WAXS, and PXRD analysis. Furthermore, along the *a*-axis, the array also showed obvious uniform spacings of 2.2 and 3.5 Å (Figure 4c), in accordance with the TEM images and *d*

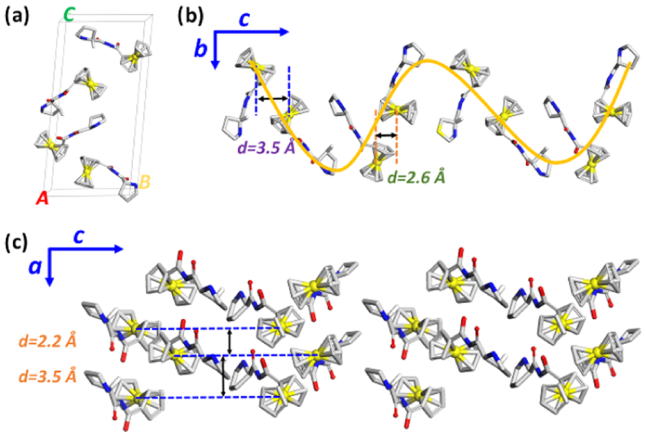

Figure 4. Proposed supramolecular packing of Fc-CO-NH-P within the nanoflowers. (a) Cell of the Fc-CO-NH-P molecules: a = 5.63 Å, b = 11.52 Å, c = 23.21 Å, α = 82.08°, β = 88.07°, and γ = 87.98°. (b) Along the *c*-axis, the ferrocene groups showed a chiral arrangement and aligned as a uniform array. The *d* spacings were measured as 2.6 and 3.5 Å. (c) Along the *a*-axis, the array also showed uniform distances of 2.2 and 3.5 Å.

spacings of WAXS results. Besides, our DFT calculations predicted that the cohesive energy (ΔE) was −127.13 kcal mol^{-1} (−1002.20 eV − 4*(−249.22 eV)), implying that the constructed model was highly stable.

The catalytic activity of various supramolecular nanostructures toward the direct aldol reaction of cyclohexanone with *p*-nitrobenzaldehyde was evaluated (Table 1 and Scheme S2). All reactions were carried out in aqueous media, with the aldehyde, 10-fold excess of ketone, and 10% catalysts loading level. We studied the catalytic activity using various nanostructures as catalysts. P6, N6, N7, and N9 did not exhibit any catalytic activity (Figure S12). On comparing their

Table 1. Fc-CO-NH-P Nanostructure-Catalyzed Aldol Reaction at Different Self-Assembly Times and Reaction Temperatures

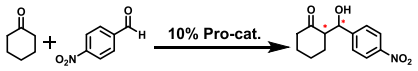

entry	catalyst	self-assembly time	yield (%)[a]	dr [anti/syn][b]	ee (%)[c]
1[d]	P7	24 h	78	69:31	91
2[d]	P9	24 h	>99	72:28	93
*3[d]	P12	24 h	>99	97:3	>99
4[d]	N12	24 h	>99	94:6	95
5[d]	P7	5 min	71	74:26	81
6[d]	P9	5 min	94	75:25	82
7[d]	P12	5 min	>99	89:11	82
8[d]	N12	5 min	>99	77:23	86
9[d]	P7	24 h	75	60:40	84
10[e]	P9	24 h	95	72:28	84
11[e]	P12	24 h	>99	93:7	92
12[e]	N12	24 h	>99	76:24	87

[a]The yield was calculated by comparing the area of the peaks located at 8.1 and 8.3 ppm in ^{1}H NMR analysis. [b]The anti/syn ratio was determined by comparing the area of the peaks located at 5.5 and 4.9 ppm in ^{1}H NMR analysis. [c]The ee% value was detected by high-performance liquid chromatography (HPLC) analysis with a Daicel Chiralcell AD-H column. [d]The catalytic reactions were conducted at 25 °C. [e]The catalytic reactions were conducted at 37 °C.

https://dx.doi.org/10.1021/acs.langmuir.0c01485
Langmuir XXXX, XXX, XXX−XXX

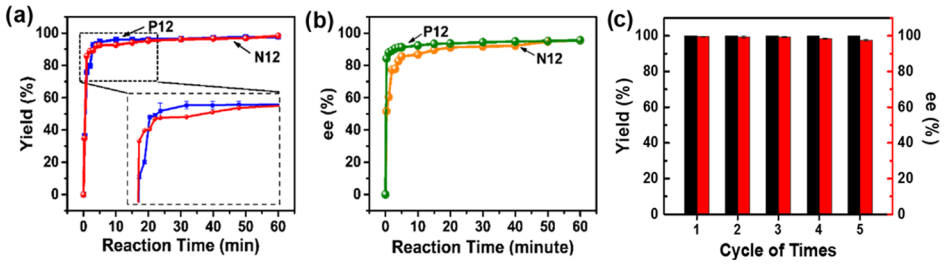

Figure 5. Kinetics (a) yield and (b) ee% of the aldol reaction in early 1 h catalyzed by P12 and N12. (c) Cyclic performance of the yield and ee% value of P12.

morphology, it was found that the unordered structures and nanospheres have no catalytic activity toward the direct aldol reaction. However, P7, P9, P12, and N12 exhibited different activities toward the aldol reaction. The yield was 78% for P7 and >99% for the other three catalysts, and the ee% value for the four catalysts was 91, 93, >99, and 95% (Table 1, entries 1−4 and Figures S13−S19), respectively. Besides, we performed an aldol reaction just catalyzed by phosphate buffer (pH 7.0, 9.0, 12.0) and sodium hydroxide solution (pH 12.0) and the yield was 0, indicating that the solution and hydroxyl ions did not possess any catalytic ability (Figures S20−S23). We also performed an aldol reaction catalyzed by L-prolinamide self-assembled in phosphate buffer and sodium hydroxide solution with a pH of 12.0. The yield was >99%, and the anti/syn ratio was detected as 27:73 and 24:76 for L-prolinamide self-assembled in phosphate buffer and sodium hydroxide solution (Figures S24 and S25), respectively. The results demonstrate the significance of ferrocene groups in high-efficiency catalysis. It was worth noting that the P12 nanoflowers exhibited the highest conversion and ee% value reported so far for the aldol reaction conducted in aqueous media. We speculated that both the fully exposed effective catalytic sites and the chiral molecular arrangement are responsible for the ultrahigh yield and stereoselectivity. On the one hand, the pyrrolidine groups located at *bc* face of the cells are exposed on the exterior of the nanosheets, which could provide large amounts of catalytic sites that are available for the aldol reaction (Figures 1f and S11). Besides, the ferrocene groups aligned regularly along the pyrrolidine groups could provide hydrophobic microenvironments and high affinity between the reactants and catalysts, thus achieving a superior yield. On the other hand, as shown in Figure 4b, the exposed catalytic sites on the nanoflowers were arranged in a chiral configuration, which could induce steric hindrance during the catalytic reactions, thus achieving high stereoselectivity.

Furthermore, we studied the effects of self-assembly time and reaction temperature on catalytic activity. We used the catalysts self-assembled for 5 min for the aldol reaction and compared with the catalysts assembled for 24 h. The yield for P12 and N12 still remained at >99%; however, the ee% value had a great drop from >99 to 82% for P12 and from 95 to 86% for N12 (Table 1, entries 7 and 8, Figures S13, S26, and S27). The downtrend was more obvious for P7 and P9; with the decrease of the self-assembly time, both the conversion and ee % decreased a lot (Table 1, entries 5 and 6, Figures S13, S28, and S29), indicating the importance of the ordered nanostructure for the high stereoselectivity toward the direct aldol reaction. Meanwhile, we investigated the effect of reaction temperature on catalytic activity. As the reaction temperature increased from normal temperature to 37 °C, although the yield remained at >99%, the ee% values decreased from close to >99 to 92% and from 95 to 87% for P12 and N12, respectively (Table 1, entries 11 and 12, Figures S13, S30, and S31). The high temperature also had a bad influence on P7 and P9. With the increase of reaction temperature, both the conversion and ee% values decreased a lot (Table 1, entries 9 and 10, Figures S13, S32 and S33). The results indicated that the catalysts assembled with sufficient time and at a relatively low temperature were preferred for the high-efficiency aldol reaction, especially high stereoselectivity.

To investigate the initial reaction rate, we selected the two excellent supramolecular catalysts, P12 and N12, which had a high yield and stereoselectivity toward the aldol reaction. In detail, we detected the products at different reaction times. Figure 5 shows the initial yield and ee% values at different times. It could be observed that at about early 5 min, N12 had a better catalytic efficiency than P12. As the reaction proceeded, the increase in yield in the reaction catalyzed by P12 was faster than that by N12. When the reaction time reached 60 min, both catalytic systems attained >99% (Figure 5a). Meanwhile, the ee% value of the two reaction systems was also observed. As Figure 5b shows, in about early 10 min, the ee% for N12 was higher than that for P12, but with the increase of time, the increase rate of the ee% value for P12 was faster than that for N12. Finally, at 60 min, the ee% for both reaction systems reached about 95%, nearly the final reaction stereoselectivity. It is worth nothing that when the reaction time reached 60 min, though the conversion and ee% value reached a high state, the anti% value was still 66% for P12 and 63% for N12 (Figures S34 and S35). We speculated that for the remaining reaction time, the catalyst action was to increase the de% value to make a single enantiomer in excess.

The ability to maintain the stability and high performance is an important characteristic of chiral catalysts. To test the cyclic performance of our prepared highly stereoselective catalyst, we used P12 to perform the next four cycles. As Figure 5c shows, after five cycles, the yield of the aldol reaction still remained at >99%, while the ee% value had a slight decrease from >99 to 97% (Figures S36−S39 and Table S1). Although the catalyst was used for five cycles, it still maintained a high performance toward the direct aldol reaction, both in yield and ee% value. This fully proved the stability and efficiency of the Fc-CO-NH-P catalyst.

CONCLUSIONS

In summary, we synthesized a simple molecule, ferrocene-L-prolinamide (Fc-CO-NH-P), which could self-assemble into versatile supramolecular nanostructures. The catalytic activity was significantly related to the self-assembled nanostructures.

https://dx.doi.org/10.1021/acs.langmuir.0c01485
Langmuir XXXX, XXX, XXX−XXX

The self-assembled nanoflowers showed a delicate 3D structure with a superior specific surface area, fully exposed catalytic sites, and chiral molecular configuration, which is expected to be used to catalyze the direct aldol reaction in aqueous media, with excellent catalytic performance, achieving both high yield (>99%) and enantioselectivity (>99%). The results can be used as a feasible new strategy for constructing nanocatalysts for asymmetric reactions through the combination of molecular design and supramolecular self-assembly.

EXPERIMENTAL SECTION

Materials and Methods. Ferrocenecarboxylic acid (Fc-COOH, 98.5% in purity), L-prolinamide (98% in purity), and anhydrous CH_2Cl_2 were obtained from Aladdin (Shanghai, China). Other chemicals were of analytical grade and were purchased from commercial sources.

Synthesis of Ferrocene-L-Prolinamide (Fc-CO-NH-P). Synthesis of chlorocarbonyl ferrocene (Scheme S1I): The reaction proceeded under anhydrous conditions. Ferrocenecarboxylic acid (300 mg, 1.3 mmol) was suspended in 100 mL of CH_2Cl_2, and after being fully dissolved, we added oxalyl chloride (220 μL, 2.6 mmol) into the solution slowly at 0 °C. After adding three drops of DMF, the mixtures continued to react at room temperature with continuous stirring for 12 h. With the increase of the reaction time, the color of the solution changed from light orange to wine red. When the reaction was completed, the sample was washed successively with HCl, $NaHCO_3$, and pure water, and CH_2Cl_2 in the organic phase was removed by mixing with anhydrous sodium sulfate and by rotary evaporation. The product with an orange color was used in the next reaction.

Synthesis of Ferrocene-L-Prolinamide (Fc-CO-NH-P) (Scheme S1II). The reaction proceeded under anhydrous conditions. L-Prolinamide (120 mg, 1.05 mmol) was dissolved in 50 mL of CH_2Cl_2, and 1.3 equiv of Et_3N (222 μL, 1.7 mmol) was added into the solution dropwise; the reactants were mixed at room temperature with stirring for 10 min and then cooled down to 0 °C in an ice bath. The previously synthesized chlorocarbonyl ferrocene was dissolved in 10 mL of anhydrous CH_2Cl_2 and then added to the mixtures dropwise; this procedure was continued for about 30 min. The reaction proceeded for 24 h at room temperature with stirring. When the reaction was completed, the sample was washed successively with HCl, $NaHCO_3$, and pure water, and CH_2Cl_2 in the organic phase was removed by rotary evaporation. Then, the product was further purified using column chromatography with 10:1 of CH_2Cl_2/CH_3OH. The yield of the two-step reaction was about 55%.

Preparation of Different pH Solutions. NaH_2PO_4 (600 mg) and $Na_2HPO_4{\cdot}12\ H_2O$ (1.79 g) were dissolved in 100 mL of H_2O, resulting in a 50 mM NaH_2PO_4 and Na_2HPO_4 solution. Phosphate buffers with a pH of 6.0, 7.0, and 9.0 were prepared by mixing a certain volume of NaH_2PO_4 and Na_2HPO_4 solution. The pH 12.0 phosphate buffer was prepared by adding a certain volume of 50 mM NaOH solution into the Na_2HPO_4 solution. The 50 mM NaOH solution was prepared by dissolving 200 mg of NaOH in 100 mL of water. By adding different volumes of HCl, the pH of the solution could be set to 6.0, 7.0, 9.0, and 12.0.

Preparation of Fc-CO-NH-P Catalysts. Different catalysts were prepared by self-assembly of Fc-CO-NH-P in various solutions. In general, we dissolved 1 mg of Fc-CO-NH-P in 1 mL of phosphate buffers (50 mM; pH 6.0, 7.0, 9.0, 12.0) at 60 °C, respectively, and the samples were moved to a 25 °C water bath to incubate for 24 h for full self-assembly. The formed catalysts were named P6, P7, P9, and P12. The same method was used to prepare catalysts in NaOH solution. We also dissolved 1 mg of Fc-CO-NH-P in 1 mL of sodium hydroxide solution (50 mM; pH 6.0, 7.0, 9.0, 12.0) at 60 °C, respectively. Then the samples were moved to a 25 °C water bath to incubate for 24 h for full self-assembly. The formed catalysts were named N6, N7, N9, and N12.

To probe the effect of the self-assembly time on the catalytic activity, we prepared another group of catalysts. In general, 1 mg of Fc-CO-NH-P was mixed with 1 mL of phosphate buffers and sodium hydroxide solution (50 mM; pH 6.0, 7.0, 9.0, 12.0) for 5 min, respectively. The mixtures were regarded as the catalysts for the control group, which were used for the aldol reaction directly.

Preparation of the L-Prolinamide Catalyst. We also dissolved 1 mg of L-prolinamide in 1 mL of phosphate buffer (50 mM, pH 12.0) and sodium hydroxide solution (50 mM, pH 12.0) at 60 °C, respectively. The samples were moved to a 25 °C water bath to incubate for 24 h for full self-assembly.

Aldol Reaction of *p*-Nitrobenzaldehyde with Cyclohexanone. An amount of 4.36 mg of *p*-nitrobenzaldehyde (0.031 mmol, 1 equiv) and 31.7 μL cyclohexanone (0.31 mmol, 10 equiv) were mixed in a vial. After adding the Fc-CO-NH-P catalysts (0.0031 mmol, 0.1 equiv), the mixtures were incubated at 25 °C for 72 h with stirring. After reaction, 1 mL of saturated NH_4Cl solution was added into the mixtures to quench the reaction, and then the mixtures were washed with 1 M HCl, 1 M $NaHCO_3$, and pure water, progressively. The organic phase was then mixed with anhydrous sodium sulfate, and then CH_2Cl_2 was taken away in a vacuum. To determine the conversion of the aldol reaction, ^{1}H NMR was used. The ee% was measured by HPLC with a Daicel Chiralcell AD-H column using the following conditions: eluent: hexane/2-PrOH = 80:20, flow rate: 0.5 mL/min, and detection λ = 254 nm.

For the control experiment, the self-assembled L-prolinamide was added into a mixture of 1.53 mg of *p*-nitrobenzaldehyde (0.011 mmol, 1 equiv) and 11.10 μL of cyclohexanone (0.11 mmol, 10 equiv) and then incubated at 25 °C for 72 h with stirring. After reaction, 1 mL of saturated NH_4Cl solution was added to the mixtures to quench the reaction, and then the mixtures were washed with 1 M HCl, 1 M $NaHCO_3$, and pure water, progressively. The organic phase was then dried with anhydrous sodium sulfate, and then taken away in a vacuum. The yield and dr values were detected by ^{1}H NMR analysis.

Cyclic Performance Test of P12. After completing the last batch of aldol reactions, the mixtures were washed with 1 M HCl, 1 M $NaHCO_3$, and pure water, progressively, and the aqueous phase was collected and centrifuged at 15 000 rpm for 20 min at 4 °C. After centrifugation, the yellow catalysts were separated at the bottom of the tube, followed by washing with pure water three times, and the final solid was used to catalyze the next batch of aldol reactions.

CHARACTERIZATION

Nuclear Magnetic Resonance Hydrogen Spectroscopy (^{1}H NMR). The samples were dissolved in $CDCl_3$ with $Si(CH_3)_4$ as the reference, and then the ^{1}H NMR spectrum was measured on an NMR spectrometer (AV-400, Bruker).

Scanning Electron Microscopy (SEM). We placed 10 μL of self-assemblies onto a glass coverslip with a diameter of 0.5 mm, and excess samples were removed. Then, the samples were air-dried, which were sputtered with platinum (E1045 Pt-coater, Hitachi High-Technologies CO., Japan). The morphology of self-assemblies was observed by SEM (S-4800, Hitachi High-Technologies CO., Japan) with an acceleration voltage of 3 keV.

Transmission Electron Microscopy (TEM). An aliquot (10 μL) of the prepared self-assemblies was put on a copper grid (200 meshes), excess self-assemblies were removed using a pipette, and then the samples were air-dried. We then investigated the morphology of the self-assemblies by TEM (JEOL 100CX-II, JEOL Ltd., Japan) with an operating voltage of 80 keV.

Atomic Force Microscopy (AFM). We extracted 100 μL aliquot of self-assemblies using a pipette, then the samples were dispersed on a mica sheet, and the samples were dried using nitrogen purging. The morphology of the self-assemblies was recorded with an atomic force microscope (AFM, Agilent 5500, Agilent).

https://dx.doi.org/10.1021/acs.langmuir.0c01485
Langmuir XXXX, XXX, XXX−XXX

Dynamic Light Scattering (DLS). The Fc-CO-NH-P nanospheres prepared in phosphate buffer (50 mM, pH 6.0) were diluted in ddH_2O and incubated at 25 °C without any disturbance for 10 min. We measured the size distribution using a Zetasizer Nano AS (Malvern Instruments, U.K.).

Fourier Transform Infrared (FTIR) Spectroscopy. At first, the self-assemblies were dried to powder using a vacuum freezing dryer, and then the samples were mixed with KBr to form pellets using a tablet machine. The infrared spectra of self-assemblies were recorded using a Nicolet-560 FTIR spectrometer (Nicolet Co.). The detection range was 400−4000 cm^{-1}, the number of scans was 16, and the resolution for each spectrum was 4 cm^{-1}.

In Situ Synchrotron Wide-Angle X-ray Diffraction (WAXD). We carried out the in situ X-ray scattering experiments of our prepared hydrogels at the 1W2A beamline of the Beijing Synchrotron Radiation Facility (Beijing, China). The wavelength of the radiation source used in the experiment was 0.154 nm, and the sample−detector (Mar165-CCD) distance was 160 mm.

Powder X-Ray Scattering Measurements. The powder XRD experiments were carried out using a PANalytical X'Pert PRO MPD (PANalytical, Netherlands); the target material was CuK (λ = 1.5406 Å). The detection angles for SAXD and WAXD were 0.5−5°and 3−40°, respectively.

Terahertz Absorption Spectroscopy (THz). We recorded THz spectra using a photoconductive switch-based Terahertz Time-Domain system at room temperature. The Terahertz system was formed by four parabolic mirrors with an 8-F confocal geometry. Our prepared self-assembled nanostructures were placed in a silicon cell, and we also used an empty cell as a reference.

Configuration Optimization. The configuration optimization of the Fc-CO-NH-P cell was performed by Materials Studio simulations, using density functional theory (DFT) calculations.

■ ASSOCIATED CONTENT

Supporting Information

The Supporting Information is available free of charge at https://pubs.acs.org/doi/10.1021/acs.langmuir.0c01485.

SEM and TEM images; X-ray diffraction patterns; circular dichroism spectra of the peptide assemblies; and HPCL data (PDF)

■ AUTHOR INFORMATION

Corresponding Author

Yuefei Wang − *State Key Laboratory of Chemical Engineering, School of Chemical Engineering and Technology and Tianjin Key Laboratory of Membrane Science and Desalination Technology, Tianjin University, Tianjin 300072, P. R. China;* orcid.org/0000-0002-5736-7431; Email: wangyuefei@tju.edu.cn

Authors

Xuejiao Yang − *State Key Laboratory of Chemical Engineering, School of Chemical Engineering and Technology, Tianjin University, Tianjin 300072, P. R. China*

Liwei Zhang − *State Key Laboratory of Chemical Engineering, School of Chemical Engineering and Technology, Tianjin University, Tianjin 300072, P. R. China*

Yaoyu Liang − *State Key Laboratory of Chemical Engineering, School of Chemical Engineering and Technology, Tianjin University, Tianjin 300072, P. R. China*

Yuhe Shen − *State Key Laboratory of Chemical Engineering, School of Chemical Engineering and Technology, Tianjin University, Tianjin 300072, P. R. China*

Qiguo Xing − *State Key Laboratory of Chemical Engineering, School of Chemical Engineering and Technology, Tianjin University, Tianjin 300072, P. R. China*

Wei Qi − *State Key Laboratory of Chemical Engineering, School of Chemical Engineering and Technology and Tianjin Key Laboratory of Membrane Science and Desalination Technology, Tianjin University, Tianjin 300072, P. R. China; Collaborative Innovation Center of Chemical Science and Engineering (Tianjin), Tianjin 300072, P. R. China;* orcid.org/0000-0002-7378-1392

Pengfei Wang − *State Key Laboratory of Precision Measuring Technology and Instruments, Tianjin University, Tianjin 30072, P. R. China*

Xiao Liu − *State Key Laboratory of Chemical Engineering, School of Chemical Engineering and Technology, Tianjin University, Tianjin 300072, P. R. China;* orcid.org/0000-0001-8077-3000

Mengyao Yang − *State Key Laboratory of Chemical Engineering, School of Chemical Engineering and Technology, Tianjin University, Tianjin 300072, P. R. China*

Rongxin Su − *State Key Laboratory of Chemical Engineering, School of Chemical Engineering and Technology and Tianjin Key Laboratory of Membrane Science and Desalination Technology, Tianjin University, Tianjin 300072, P. R. China; Collaborative Innovation Center of Chemical Science and Engineering (Tianjin), Tianjin 300072, P. R. China;* orcid.org/0000-0001-9778-9113

Mingxia He − *State Key Laboratory of Precision Measuring Technology and Instruments, Tianjin University, Tianjin 30072, P. R. China*

Zhimin He − *State Key Laboratory of Chemical Engineering, School of Chemical Engineering and Technology, Tianjin University, Tianjin 300072, P. R. China*

Complete contact information is available at: https://pubs.acs.org/10.1021/acs.langmuir.0c01485

Author Contributions

[⊥]X.Y., L.Z., and Y.L. contributed equally to this work.

Notes

The authors declare no competing financial interest.

■ ACKNOWLEDGMENTS

This work was supported by the National Natural Science Foundation of China (Nos. 21621004 and 22078239), the Tianjin Development Program for Innovation and Entrepreneurship (2018), and the State Key Laboratory of Chemical Engineering (SKL-ChE-20Z04). The authors thank Dr. Guang Mo and Prof. Zhonghua Wu of BSRF for their assistance with the WAXS measurement.

■ REFERENCES

(1) Eder, U.; Sauer, G.; Wiechert, R. New Type of Asymmetric Cyclization to Optically Active Steroid CD Partial Structures. *Angew. Chem., Int. Ed.* **1971**, *10*, 496−497.

(2) Hajos, Z. G.; Parrish, D. R. Asymmetric synthesis of bicyclic intermediates of natural product chemistry. *J. Org. Chem.* **1974**, *39*, 1615−1621.

(3) List, B.; Lerner, R. A.; Barbas, C. F. Proline-catalyzed direct asymmetric aldol reactions. *J. Am. Chem. Soc.* **2000**, *122*, 2395−2396.
(4) Notz, W.; Tanaka, F.; Barbas, C. F. Enamine-based organocatalysis with proline and diamines: The development of direct catalytic asymmetric Aldol, Mannich, Michael, and Diels-Alder reactions. *Acc. Chem. Res.* **2004**, *37*, 580−591.
(5) Chowdari, N. S.; Ramachary, D. B.; Cordova, A.; Barbas, C. F. Proline-catalyzed asymmetric assembly reactions: enzyme-like assembly of carbohydrates and polyketides from three aldehyde substrates. *Tetrahedron Lett.* **2002**, *43*, 9591−9595.
(6) Sessler, J. L.; Seidel, D.; Vivian, A. E.; Lynch, V.; Scott, B. L.; Keogh, D. W. Hexaphyrin(1.0.1.0.0.0): An expanded porphyrin ligand for the actinide cations uranyl (UO22+) and neptunyl (NpO2+). *Angew. Chem., Int. Ed.* **2001**, *40*, 591−594.
(7) Enders, D.; Grondal, C.; Huttl, M. R. M. Asymmetric organocatalytic domino reactions. *Angew. Chem., Int. Ed.* **2007**, *46*, 1570−1581.
(8) Berkessel, A.; Grorer, H. *Asymmetric Organocatalysis - From Biomimetic Concepts to Powerful Methods for Asymmetric Synthesis*; Wiley-VCH: Weinheim, 2005; pp 1−8.
(9) Mase, N.; Barbas, C. F. In water, on water, and by water: mimicking nature's aldolases with organocatalysis and water. *Org. Biomol. Chem.* **2010**, *8*, 4043−4050.
(10) Mase, N.; Nakai, Y.; Ohara, N.; Yoda, H.; Takabe, K.; Tanaka, F.; Barbas, C. F. Organocatalytic direct asymmetric aldol reactions in water. *J. Am. Chem. Soc.* **2006**, *128*, 734−735.
(11) Hayashi, Y.; Sumiya, T.; Takahashi, J.; Gotoh, H.; Urushima, T.; Shoji, M. Highly diastereo- and enantioselective direct aldol reactions in water. *Angew. Chem., Int. Ed.* **2006**, *45*, 958−961.
(12) Gruttadauria, M.; Giacalone, F.; Noto, R. Water in Stereoselective Organocatalytic Reactions. *Adv. Synth. Catal.* **2009**, *351*, 33−57.
(13) Moyano, A.; Rios, R. Asymmetric Organocatalytic Cyclization and Cycloaddition Reactions. *Chem. Rev.* **2011**, *111*, 4703−4832.
(14) Scheffler, U.; Mahrwald, R. Recent advances in organocatalytic methods for asymmetric C-C bond formation. *Chem. - Eur. J.* **2013**, *19*, 14346−14396.
(15) Volla, C. M. R.; Atodiresei, L.; Rueping, M. Catalytic C-C Bond-Forming Multi-Component Cascade or Domino Reactions: Pushing the Boundaries of Complexity in Asymmetric Organocatalysis. *Chem. Rev.* **2014**, *114*, 2390−2431.
(16) Dai, L. X.; Tu, T.; You, S. L.; Deng, W. P.; Hou, X. L. Asymmetric catalysis with chiral ferrocene ligands. *Acc. Chem. Res.* **2003**, *36*, 659−667.
(17) Gómez Arrayás, R.; Adrio, J.; Carretero, J. C. Recent applications of chiral ferrocene ligands in asymmetric catalysis. *Angew. Chem., Int. Ed.* **2006**, *45*, 7674−7715.
(18) Roelfes, G.; Feringa, B. L. DNA-based asymmetric catalysis. *Angew. Chem., Int. Ed.* **2005**, *44*, 3230−3232.
(19) Boersma, A. J.; Megens, R. P.; Feringa, B. L.; Roelfes, G. DNA-based asymmetric catalysis. *Chem. Soc. Rev.* **2010**, *39*, 2083−2092.
(20) Tang, Z.; Marx, A. Proline-modified DNA as catalyst of the aldol reaction. *Angew. Chem., Int. Ed.* **2007**, *46*, 7297−7300.
(21) Akagawa, K.; Sakamoto, S.; Kudo, K. Direct asymmetric aldol reaction in aqueous media using polymer-supported peptide. *Tetrahedron Lett.* **2005**, *46*, 8185−8187.
(22) Zayas, H. A.; Lu, A.; Valade, D.; Amir, F.; Jia, Z. F.; O'Reilly, R. K.; Monteiro, M. J. Thermoresponsive Polymer-Supported L-Proline Micelle Catalysts for the Direct Asymmetric Aldol Reaction in Water. *ACS Macro Lett.* **2013**, *2*, 327−331.
(23) Lu, A.; Moatsou, D.; Longbottom, D. A.; O'Reilly, R. K. Tuning the catalytic activity of L-proline functionalized hydrophobic nanogel particles in water. *Chem. Sci.* **2013**, *4*, 965−969.
(24) Gao, J. S.; Liu, J.; Bai, S. Y.; Wang, P. Y.; Zhong, H.; Yang, Q. H.; Li, C. The nanocomposites of SO_3H-hollow-nanosphere and chiral amine for asymmetric aldol reaction. *J. Mater. Chem.* **2009**, *19*, 8580−8588.
(25) Kaushik, M.; Basu, K.; Benoit, C.; Cirtiu, C. M.; Vali, H.; Moores, A. Cellulose Nanocrystals as Chiral Inducers: Enantioselective Catalysis and Transmission Electron Microscopy 3D Characterization. *J. Am. Chem. Soc.* **2015**, *137*, 6124−6127.
(26) Seo, J. S.; Whang, D.; Lee, H.; Jun, S. I.; Oh, J.; Jeon, Y. J.; Kim, K. A homochiral metal-organic porous material for enantioselective separation and catalysis. *Nature* **2000**, *404*, 982−986.
(27) Ma, L. Q.; Abney, C.; Lin, W. B. Enantioselective catalysis with homochiral metal-organic frameworks. *Chem. Soc. Rev.* **2009**, *38*, 1248−1256.
(28) Meeuwissen, J.; Reek, J. N. H. Supramolecular catalysis beyond enzyme mimics. *Nat. Chem.* **2010**, *2*, 615−621.
(29) Jiang, J.; Meng, Y.; Zhang, L.; Liu, M. H. Self-Assembled Single-Walled Metal-Helical Nanotube (M-HN): Creation of Efficient Supramolecular Catalysts for Asymmetric Reaction. *J. Am. Chem. Soc.* **2016**, *138*, 15629−15635.
(30) Singh, N.; Zhang, K.; Angulo-Pachon, C. A.; Mendes, E.; van Esch, J. H.; Escuder, B. Tandem reactions in self-sorted catalytic molecular hydrogels. *Chem. Sci.* **2016**, *7*, 5568−5572.
(31) Lee, K. S.; Parquette, J. R. A self-assembled nanotube for the direct aldol reaction in water. *Chem. Commun.* **2015**, *51*, 15653−15656.
(32) Tena-Solsona, M.; Nanda, J.; Diaz-Oltra, S.; Chotera, A.; Ashkenasy, G.; Escuder, B. Emergent Catalytic Behavior of Self-Assembled Low Molecular Weight Peptide-Based Aggregates and Hydrogels. *Chem. - Eur. J.* **2016**, *22*, 6687−6694.
(33) Rodriguez-Llansola, F.; Escuder, B.; Miravet, J. F. Switchable Performance of an L-Proline-Derived Basic Catalyst Controlled by Supramolecular Gelation. *J. Am. Chem. Soc.* **2009**, *131*, 11478−11484.
(34) Qin, L.; Zhang, L.; Jin, Q.; Zhang, J.; Han, B.; Liu, M. Supramolecular Assemblies of Amphiphilic L-Proline Regulated by Compressed CO_2 as a Recyclable Organocatalyst for the Asymmetric Aldol Reaction. *Angew. Chem., Int. Ed.* **2013**, *52*, 7761−7765.
(35) Gu, X.; Bi, S.; Guo, L.; Zhao, Y.; Li, T.; Liu, M.; Chen, P.; Wu, Y. Facile Fabrication of Ordered Component-Tunable Heterobimetallic Self-Assembly Nanosheet for Catalyzing "Click" Reaction. *ACS Omega* **2017**, *2*, 5415−5433.
(36) Sun, Z. F.; Li, Z. Y.; He, Y. H.; Shen, R. J.; Deng, L.; Yang, M. H.; Liang, Y. Z.; Zhang, Y. Ferrocenoyl Phenylalanine: A New Strategy Toward Supramolecular Hydrogels with Multistimuli Responsive Properties. *J. Am. Chem. Soc.* **2013**, *135*, 13379−13386.
(37) Wang, Y. F.; Qi, W.; Huang, R. L.; Yang, X. J.; Wang, M. F.; Su, R. X.; He, Z. M. Rational Design of Chiral Nanostructures from Self-Assembly of a Ferrocene-Modified Dipeptide. *J. Am. Chem. Soc.* **2015**, *137*, 7869−7880.
(38) Yang, X. J.; Wang, Y. F.; Qi, W.; Su, R. X.; He, Z. M. Bioorganometallic ferrocene-tripeptide nanoemulsions. *Nanoscale* **2017**, *9*, 15323−15331.
(39) Yang, X. J.; Wang, Y. F.; Qi, W.; Zhang, J. X.; Zhang, L. W.; Huang, R. L.; Su, R. X.; He, Z. M. Photo-Induced Polymerization and Reconfigurable Assembly of Multifunctional Ferrocene-Tyrosine. *Small* **2018**, *14*, No. 1800772.
(40) Kirschner, D. A.; Abraham, C.; Selkoe, D. J. X-ray diffraction from intraneuronal paired helical filaments and extraneuronal amyloid fibers in Alzheimer disease indicates cross-beta conformation. *Proc. Natl. Acad. Sci. U.S.A.* **1986**, *83*, 503−507.
(41) Cui, H. G.; Cheetham, A. G.; Pashuck, E. T.; Stupp, S. I. Amino Acid Sequence in Constitutionally Isomeric Tetrapeptide Amphiphiles Dictates Architecture of One-Dimensional Nanostructures. *J. Am. Chem. Soc.* **2014**, *136*, 12461−12468.
(42) Nguyen, J. T.; Inouye, H.; Baldwin, M. A.; Fletterick, R. J.; Cohen, F. E.; Prusiner, S. B.; Kirschner, D. A. X-ray diffraction of scrapie prion rods and PrP peptides. *J. Mol. Biol.* **1995**, *252*, 412−422.
(43) Makin, O. S.; Serpell, L. C. Structures for amyloid fibrils. *FEBS J.* **2005**, *272*, 5950−5961.
(44) Kutteruf, M. R.; Brown, C. M.; Iwaki, L. K.; Campbell, M. B.; Korter, T. M.; Heilweil, E. J. Terahertz spectroscopy of short-chain polypeptides. *Chem. Phys. Lett.* **2003**, *375*, 337−343.
(45) Yamamoto, K.; Tominaga, K.; Sasakawa, H.; Tamura, A.; Murakami, H.; Ohtake, H.; Sarukura, N. Terahertz time-domain

https://dx.doi.org/10.1021/acs.langmuir.0c01485
Langmuir XXXX, XXX, XXX−XXX

spectroscopy of amino acids and polypeptides. *Biophys. J.* **2005**, *89*, L22−L24.
(46) Shen, S. C.; Santo, L.; Genzel, L. THz spectra for some biomolecules. *Int. J. Infrared Millimeter Waves* **2007**, *28*, 595−610.
(47) Pan, T.; Li, S.; Zou, T.; Yu, Z.; Zhang, B.; Wang, C.; Zhang, J.; He, M.; Zhao, H. Terahertz spectra of l-phenylalanine and its monohydrate. *Spectrochim. Acta, Part A* **2017**, *178*, 19−23.
(48) Lara, C.; Reynolds, N. P.; Berryman, J. T.; Xu, A. Q.; Zhang, A. F.; Mezzenga, R. ILQINS Hexapeptide, Identified in Lysozyme Left-Handed Helical Ribbons and Nanotubes, Forms Right-Handed Helical Ribbons and Crystals. *J. Am. Chem. Soc.* **2014**, *136*, 4732−4739.

https://dx.doi.org/10.1021/acs.langmuir.0c01485
Langmuir XXXX, XXX, XXX−XXX